Two- and Three-Body Dissociation Dynamics of Temporary Negative Ion NF3()

ARTICLE *in* THE JOURNAL OF PHYSICAL CHEMISTRY A · MARCH 2013

Impact Factor: 2.69 · DOI: 10.1021/jp400026c · Source: PubMed

4 AUTHORS, INCLUDING:

Lei Xia

14 PUBLICATIONS **52** CITATIONS

SEE PROFILE

Shan Xi Tian

University of Science and Technology of China

88 PUBLICATIONS **713** CITATIONS

SEE PROFILE

THE JOURNAL OF PHYSICAL CHEMISTRY A

Article

pubs.acs.org/JPCA

Two- and Three-Body Dissociation Dynamics of Temporary Negative Ion NF_3^-

Hong-Kai Li, Lei Xia, Xian-Jin Zeng, and Shan Xi Tian*

Hefei National Laboratory for Physical Sciences at the Microscale and Department of Chemical Physics, University of Science and Technology of China, Hefei, Anhui 230026, China

ABSTRACT: Dissociation dynamics of temporary negative ion NF_3^- formed in the low-energy (0.5 to 4.5 eV) electron attachment is investigated by the anion velocity slice imaging spectroscopy. The kinetic and angular distributions of the F^- fragment indicate that this fragment is produced via two distinctly different dissociation channels, namely, two-body and three-body fragmentations, at the higher electron attachment energies. The anisotropic distributions of the fast F^- ions are interpreted as the two-body dissociations relevant to the ^2E resonant state of NF_3^-, whereas the slow F^- can be produced via various three-body dissociations with the products of $NF(X\ ^3\Sigma^-) + F + F^-$, $NF(b\ ^1\Sigma^+) + F + F^-$, or $N + F_2 + F^-$, depending on the electron attachment energy.

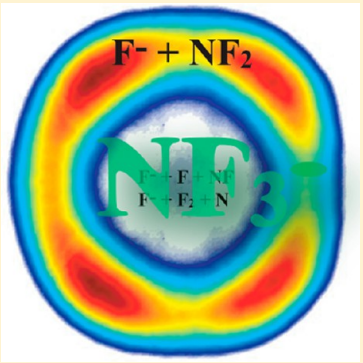

1. INTRODUCTION

An electron can be captured by a molecule particularly at the low collision energy. After quick redistribution of the electron excess energy among the internal degrees of freedom of the temporary negative ion (TNI) species formed by electron capture or attachment, the TNI may decompose via various dissociative channels that are competitive with electron autodetachment.[1] Measurements of the angular and kinetic energy distributions of the fragments produced in the above dissociative electron attachment (DEA) process can directly provide information about the excess energy redistribution in the TNI and the subsequent energy partition among the fragments.[2−6] Such e experimental studies can also be a testing ground for the few-body kinetic correlation problem. The few-body problem as an important unsolved problem in physics continually receives much attention through study of the multibody fragmentation (a typical model) in the molecular collision and photoabsorption.[7,8] Although the three-body dissociations were proposed in some DEA processes of different molecules,[2−6] until now there has been only one comprehensive theoretical study on the dominance of the three-body dissociation for the observed O^- cross sections in the DEA to H_2O,[9] but it lacks the factual experimental evidence. In this work, the DEA processes of molecule nitrogen trifluoride (NF_3) in the low electron energy range of 0.5 to 4.5 eV are investigated with the anion velocity slice imaging technique.[10] We demonstrate that the three-body and two-body dissociations lead to the slow and fast F^- fragments, respectively.

Electron-NF_3 scattering has been extensively studied[3−5,11−13] because the related elastic and inelastic scattering and reactions are the important processes in low-temperature plasma and NF_3 is widely applied in plasma etching technology.[14] In the low-energy electron collisions, two low-lying resonant states were identified around 1.7 to 1.8 eV (NF_3^-, ^2E) and 2.2 to 3.0 eV (NF_3^{*-}, $^2A_1$).[4,5,11−13] According to the kinetic energies of the F^- fragment estimated by the "direct" and "turn-back" flight-time differences measured by using the linear time-of-flight ion mass spectrometer, two types of the F^- fragment, the fast and slow, were found and suspected to be via the two-body ($NF_2 + F^-$) and three-body ($NF + F + F^-$) dissociation channels,[4,5] respectively. This conjecture requires further examination by using the present more sophisticated experimental technique. More importantly, the spatial distribution of the F^- fragment is still unavailable, but it is essential to reveal the stereodynamics of the subreactions induced by the F^- fragment. Furthermore, fluorination effects have been characterized by the differences between the total cross sections of electron collision with hydrocarbons and the corresponding fluorocarbons. (See ref 13 and the references cited within.) This work will also let us have more insight into the perfluorination effect on the DEA through comparison with a recent work for NH_3 by Ram and Krishnakumar.[6]

2. EXPERIMENTAL METHOD

The DEA experiments for the gas-phase molecule NF_3 (the commercial sample is of purity higher than 99%) have been done at the eight selected electron energies, 0.5, 1.0, 1.8, 2.3, 2.8, 3.2, 4.0, and 4.5 eV, by using our anion velocity slice imaging apparatus. The details of this apparatus can be found in ref 10. In brief, an effusive molecular beam of the sample (along y axis) was perpendicular to the pulsed electron beam (along

Received: January 2, 2013
Revised: March 18, 2013
Published: March 26, 2013

   dx.doi.org/10.1021/jp400026c | J. Phys. Chem. A 2013, 117, 3176−3182

Table 1. Energetics of the Different Dissociation Channels into F^- Fragment[a]

dissociation channel	thermodynamic threshold (eV)
NF_2 ($X\ ^2B_1$) + F^-	−0.88 (exptl),[b] −0.83 ± 0.12,[b] −0.93 ± 0.02,[c] −0.94[d]
NF_2* ($A\ ^2A_1$) + F^-	2.94[e]
NF ($X\ ^3\Sigma^-$) + F + F^-	1.9,[c] 2.09[e]
NF* ($b\ ^1\Sigma^+$) + F + F^-	4.33[e]
N + F_2 + F^-	3.7,[b] 3.59[e]
N + 2F + F^-	5.3,[b] 5.19[e]
NF_2^+ + F^-	10.55[e]

[a]Species without the state notations are at the electronic ground states. [b]Ref 3. [c]Ref 5. [d]Ref 19. [e]Ref 15 and using the electron affinity value of fluorine atom 3.401 eV.

the x axis) that was emitted from a homemade electron gun (the thermal energy spread of ∼0.5 eV) and collimated with the homogeneous magnetic field produced by a pair of Helmholtz coils. The F^- ions produced in the DEA (the other source, e.g., the ion-pair dissociation $e^- + NF_3 \rightarrow F^- + NF_2^+ + e'^-$, can be ruled out because of its higher energetic threshold ca. 10.55 eV, see Table 1 and ref 15) were periodically pushed out of the reaction area and then allowed to pass through the time-of-flight tube (along the y axis). The F^- ions produced in one electron pulse expanded to form a Newton sphere by the space and velocity focusing.[10] The 3D momentum distributions of the F^- ions were detected with a triplet set of microchannel plates and a phosphor screen. Each time-sliced image of F^- ions, that is, the central sliced sheet (in the x−z plane) of the Newton sphere, was recorded with a CCD camera and by the application of a narrow time-gate pulse voltage on the last microchannel plate. The effective width of this time-gate pulse was ∼45 ns, which was acceptable for slicing the Newton sphere of the F^- ion with the time-of-flight spread of ∼430 ns. The kinetic energies derived from the image have been calibrated with the experimental data available in the literature.[10,16−18]

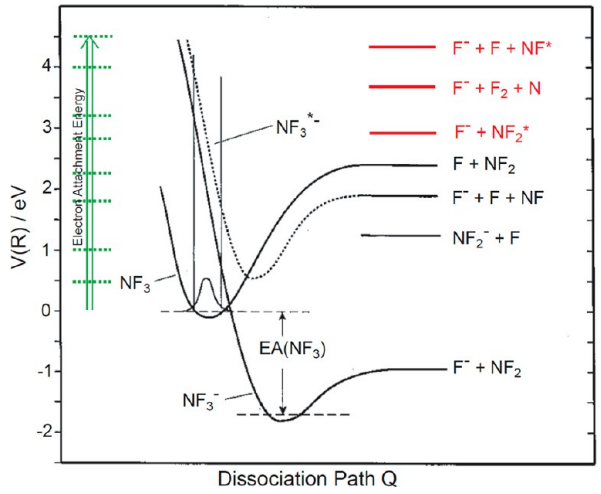

Figure 1. Schematic potential-energy diagrams relevant for DEA process of NF_3 (adapted from ref 5 and modified in this work). In the Franck−Condon region, NF_3^- is at the ^2E resonant state; NF_3^{*-} is at the $^2A_1$ resonant state. The energy ladder (green dotted lines) in the left represents the electron attachment energies investigated in this work.

3. RESULTS AND DISCUSSION

3.1. Sliced Images. In the anion mass spectroscopy studies, three types of the negatively charged fragments, F^-, F_2^-, and NF_2^-, were detected.[3−5] The cross-section ratio $\sigma(F^-)$:$\sigma(F_2^-)$:$\sigma(NF_2^-)$ was recently determined to be $1:10^{-3}:10^{-4}$ (ref 4). It is unfeasible to investigate the dissociation dynamics for the minors (F_2^- and NF_2^-) in this work because of the much smaller cross sections of these fragments and the low sample intensity. (The working background pressure was $\sim10^{-5}$ Pa.) The thermochemistry values of the TNI (estimated using the data from refs 3, 5, 15, and 19) as well as the ion-pair dissociation threshold of the neutral[15] are listed in Table 1. Some of them are implemented in Figure 1, which was originally given in ref 5. In the vertical attachments at the eight different energies (assigned with green dotted lines in Figure 1), five dissociation paths to F^- should be considered. Because the large positive electron affinity (EA) of NF_3, the stable NF_3^- is 1.71 eV lower in energy than the neutral.[5] The lowest DEA channel to the electronic ground-state species F^- and NF_2 is exothermic. It is noted that the asymptotic dissociations are detected in the experiments, whereas the resonant states of TNI NF_3^- are formed in Franck−Condon transitions by the vertical attachment. With the increase in the electron attachment energy, the transitions can reach the different sites on the repulsive wall of the potential energy curves of NF_3^-, leading to the spontaneous dissociations within different time scales. This will be exhibited as the pattern changes of the F^- sliced images recorded at the different electron energies.

The sliced images of F^- fragment recorded at the first six attachment energies are depicted in Figure 2, whereas those at 4.0 and 4.5 eV are shown in Figure 3. The ion intensities are normalized, respectively, in each image. The larger image size indicates the higher F^- momentum or velocity value. Besides the faster F^- anions (shown as four petals in the outer circle), the slower F^- anions are also observed as the central signals in the images at 1.8, 2.3, 2.8, 3.2, and 4.0 eV. The present results are in agreement with the previous conclusion derived from the linear time-of-flight mass spectroscopy experiments.[4,5] According to the working principle of the ion velocity slice imaging technique, the Newton sphere of such slow F^- approaching the detector should be too small to be sliced by using the present slicing time-gate (∼45 ns).[10] To observe more clearly the angular distribution of these slow F^- ions, we zoom in on the images at 4.0 and 4.5 eV in a proportion by biasing the electrode voltages (as done in our previous work[18]). However, due to the limited size of our ion detector (its effective diameter is 40 mm), as shown in the upper right and bottom panels of Figure 3, the signals of the faster F^- ion are partially lost under the zooming-in experimental conditions.

In Figures 2 and 3, the electron incident direction is from left to right and through the central of the images. Obviously, one can find that the fast F^- anions prefer a little more in the

dx.doi.org/10.1021/jp400026c | J. Phys. Chem. A 2013, 117, 3176−3182

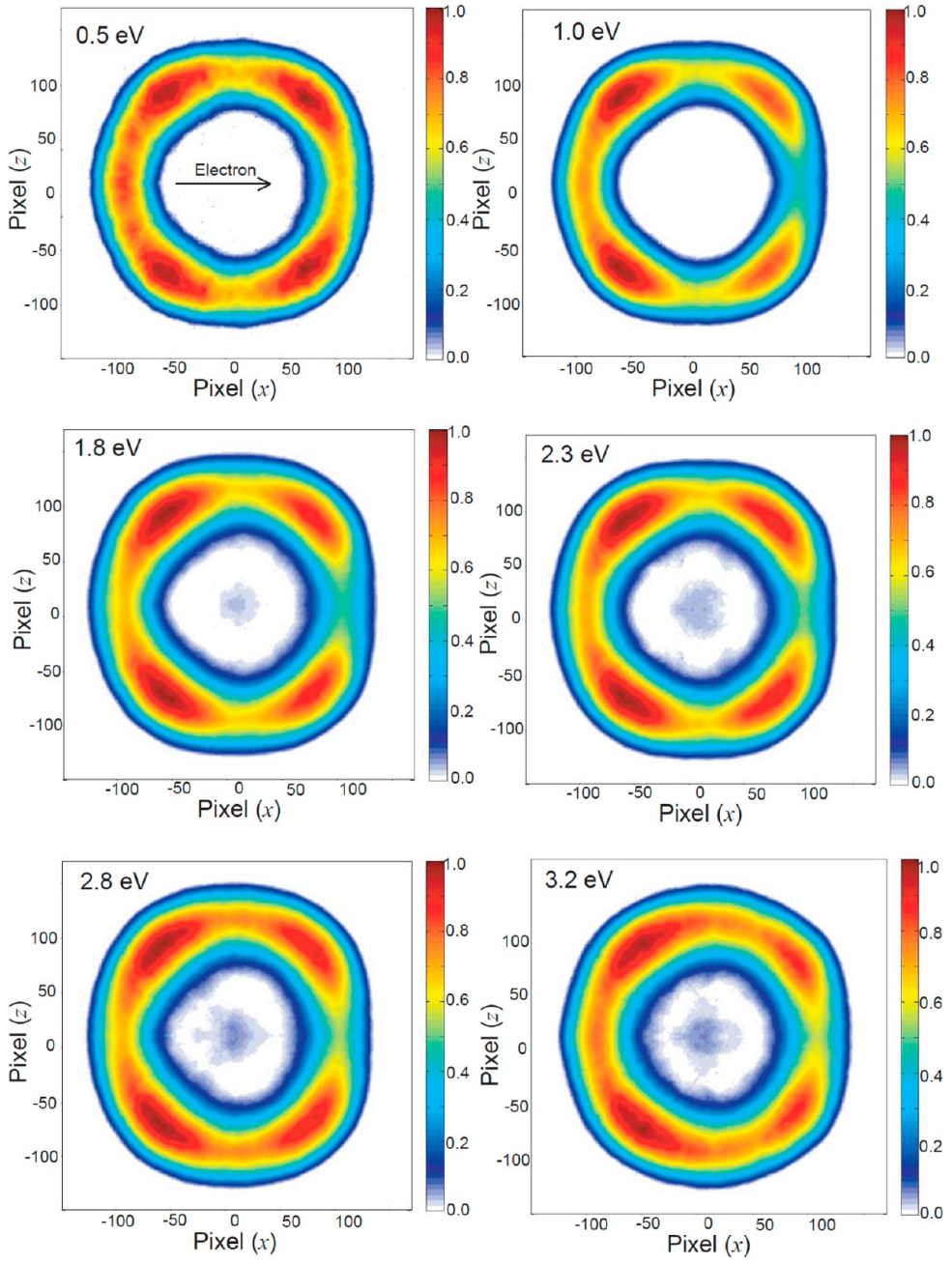

Figure 2. Sliced images of F^- fragment produced at the different electron attachment energies. The electron incident direction is shown as an arrow in the upper left panel (at 0.5 eV). The ion intensity in each image is normalized, respectively.

backward scattering direction (θ = 180°) than the forward direction (θ = 0°) besides the tetrad-petal distributions perpendicular to the electron incident direction. The slow F^- anions observed as the central isotropic distributions at 1.8 and 2.3 eV can be confidently attributed to the three-body dissociation to $NF(X\ ^3\Sigma^-) + F + F^-$ because its thermochemistry threshold is about 1.9[5] or 2.09 eV.[15] (See Table 1 and Figure 1.) Because of the thermal energy spread of the incident electron beam (0.5 eV), we can also observe this dissociation at 1.8 eV. At the high electron energies of 2.8 and 3.2 eV, another two-body dissociation with yields of the electronic ground-state F^- and the electronic excited-state NF_2^* ($A\ ^2A_1$) is energetically accessed in principle. The other three-body dissociations to $N + F_2 + F^-$ (threshold ~3.7 eV[3] or 3.59 eV[15]) and to NF^* ($b\ ^1\Sigma^+$) + F + F^- (threshold~ 4.33 eV[15]) may join at the higher electron energies 4.0 and 4.5 eV. The four-body dissociation to N + 2F + F^- is ignored in the present study due to its too high threshold. Although the kinetic energy of the slow F^- produced at the electron energies 4.0 and 4.5 eV is quite small (<0.1 eV estimated from the images in Figure 3), the angular distributions are slightly anisotropic. At the same energy of 4.0 eV (see the upper panels of Figure 3) the anisotropic distributions of the slow F^- show some differences that may arise from two factors: (1) In the left image almost a full Newton sphere (not a slice) of the slow F^- is projected onto the detector, while the right image may be a pseudo sliced image. For the latter, the time-gate width of ca. 45 ns[10] is still too wide to be used in slicing the enlarged Newton sphere of the slow F^- because this sphere may still be small. (2) The sliced images must be extremely sensitive to the

dx.doi.org/10.1021/jp400026c | J. Phys. Chem. A 2013, 117, 3176−3182

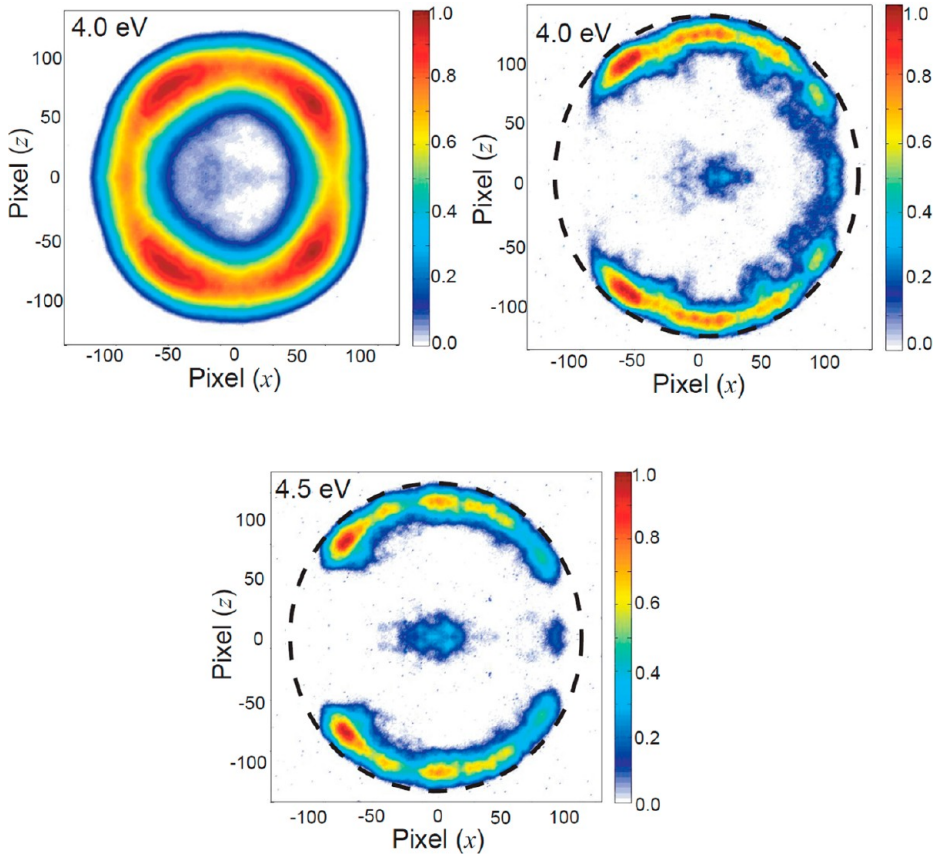

Figure 3. Sliced images of F^- fragment produced at the electron attachment energies 4.0 and 4.5 eV. The images in the upper right and bottom panels were recorded under the zooming-in conditions by applying the lower voltages, and the black dotted circles represent the effective size of the detector. The electron incident direction is the same as shown in Figure 2. The ion intensity in each image is normalized, respectively.

arising position and pulse shape of the time gate used. In fact, we have some uncertainty or instability of the voltage pulse (less than several nanoseconds) during the experiments. The difference about the anisotropic distributions between the slow F^- at 4.0 eV and that at 4.5 eV may arise from the different contributions of various three-body dissociation channels discussed above; moreover, more and more dissociations will be involved at the higher electron energies. However, the predominance of each channel at these electron energies cannot be further determined, only when the complete experiments, for example, the anion-neutral fragment coincidence,[7] are applicable.

3.2. Kinetic Energy Distributions. The kinetic energy distributions of the F^- fragment are plotted in Figure 4, and the slow and fast F^- can be clearly observed. At the electron energies of 0.5, 1.0, and 1.8 eV, the kinetic energy of the F^- fragment extends to the value higher than the respective electron energy. This indicates that the translational energies of fragments are partially from the energy release of the exothermic DEA process $e^- + NF_3 \rightarrow NF_2(X\ ^2B_1) + F^-$. No significant increases in the kinetic energy of the fast F^- are observed in Figure 4. In the previous experimental studies, the distinctly different slopes of the kinetic energy of F^- in terms of the electron energy were reported.[4,5] The kinetic energy of the fast F^- was estimated to be ~0.5 eV,[4] whereas it was 1.1 eV[5] at the same electron energy 0.8 eV. In general, the present results are much closer to those obtained by Ruckhaberle et al.[5] They suggested that about half of the electron energy should be transformed into the translational energy of the products.[5]

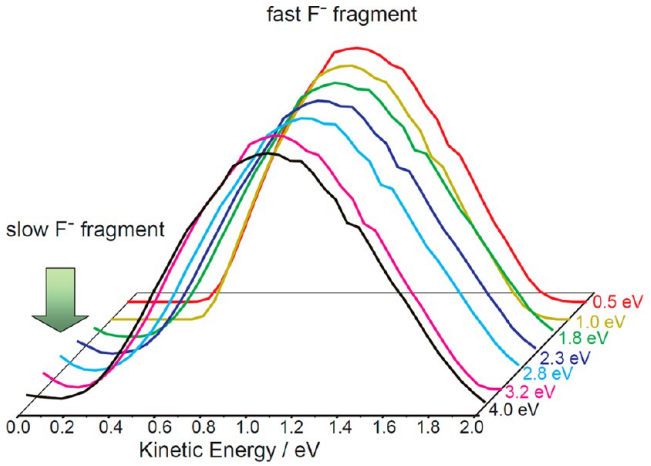

Figure 4. Kinetic energy distributions of F^- at the different electron attachment energies. The ion intensity is normalized, respectively, at different electron energies.

Within momentum and energy conservations, the total kinetic energy (E_k) can be estimated as[20]

$$E_k = E_k^i \frac{M}{m} - \frac{3}{2}RT\frac{m_i}{m} \quad (1)$$

where E_k^i is the measured kinetic energy of anion; M, m, and m_i are the masses of the parent molecule, neutral fragment (NF_2), and anionic fragment (F^-), respectively; R is the gas constant; and T is the gas-sample temperature. At the low electron

dx.doi.org/10.1021/jp400026c | J. Phys. Chem. A 2013, 117, 3176−3182

energies 0.5 and 1.0 eV, almost all electron energy together with the energy released from the exothermic dissociation is efficiently converted into the kinetic energy of the fragments. Whereas at the electron energy of 1.8 eV the maximum kinetic energy of the fast F^- is ~1.10 eV, correspondingly the total kinetic energy E_k is 1.43 eV. This E_k value is comparable to the residual energy 1.27 eV, whereas the latter may be transformed into the internal excitation (vibrational and rotational) of the NF_2 fragment. Because of the poor energy resolution (~0.5 eV) of the electron beam, we are unable to see distinct rings in the image if the F^- fragment is produced together with the vibrational excited-state NF_2. At the electron energy 3.2 eV, the dissociation to NF_2^* ($A\ ^2A_1$) + F^- may be ignored because it leads to $E_k^i(F^-) \approx 0.19$ eV, whereas in Figure 4 the relative F^- intensity at this kinetic energy is extremely low. However, the NF_2^* ($A\ ^2A_1$) at vibrationally excited states could be produced, leading to the lower kinetic energies of F^-. In the following text, we will discuss the angular distributions of the fast F^-.

3.3. Angular Distributions. To elucidate the angular distribution of anionic fragments produced in the DEA process, the formula of the differential cross section derived by Tronc et al. is frequently used[21]

$$\sigma_{DEA} \propto |\sum_{l=\mu}^{\infty} i^l e^{i\delta_l} a(k)_{l\mu} Y_{l\mu}(\Omega)|^2 \quad (2)$$

where k is the impinging electron wave vector and the impinging wave is further expressed with partial waves of the different angular momentum l ($l \geq |\mu|$), Ω is the scattering direction of the fragment ion, $a(k)_{l\mu}$ is an energy-dependent expansion coefficient, and $Y_{l\mu}$ is spherical harmonics related to the initial (neutral) and final (resonant anion) states. $|\mu|$ equals $|\Lambda_f - \Lambda_i|$, representing the difference in the projection of the angular momentum along the internuclear axis for the neutral and resonant anion. In the formation of a resonant state, the different influences on each partial wave of the impinging electron by the interaction potential of the target result in the phase lags (δ_l) among these partial waves. Equation 2 is based on the pure resonant scattering-potential scattering approximation and originated from the theory of O'Malley and Taylor[22] and the symmetry arguments of Dunn.[23] Although this equation is only suitable for diatomic molecules, it can still be justifiable to use this diatomic approximation for polyatomic molecules if the dissociation is along the center of mass axis of the molecule and the dominant portion of the energy released going into translational motion of the fragments is along the molecular axis.[6,24]

As pointed out in the previous theoretical studies,[12,13] the lowest resonant state ^2E of NF_3^- is of the electronic configuration $...(1a_2)^2(4a_1)^2(5e)^1$, where the impinging electron is captured at the double-degenerate 5e orbital (the lowest unoccupied molecular orbital (LUMO)) of the neutral. In Figure 5, the nodal planes along the N−F bond in the electron density maps of this orbital and the next LUMO (LUMO+1) $5a_1$ clearly indicate the antibond σ^* (N−F) characters. The previous conjecture about the role of the next resonant state $^2A_1$ with the electron configuration $...(1a_2)^2(4a_1)^2(5a_1)^1$ in the DEA process[12] is clarified here. The resonant-state energies were determined to be 1.7 to 1.8 eV (NF_3^-, ^2E) and 2.2 to 3.0 eV ($NF_3{}^{*-}$, $^2A_1$),[4,5,11−13] implying that these two states should be related to the two-body and three-body dissociations.

In contrast with the fragmentation from CF_3Cl^- to Cl^- along the molecular C_3 symmetry axis,[23] the two-body dissociation

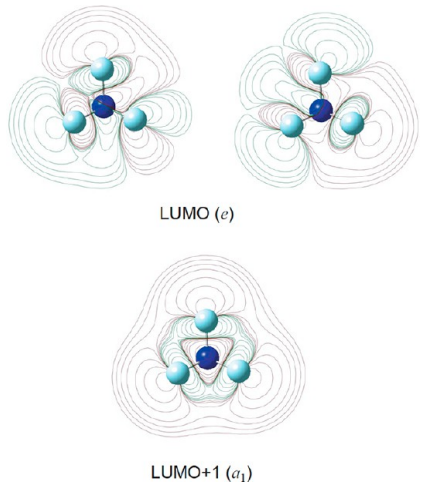

Figure 5. Electron counter maps of the LUMO (double degenerate, e) and the next LUMO (LUMO+1, a_1) of the neutral NF_3.

yielding F^- cannot be simply treated as the dissociation of a quasi-diatomic molecule (NF_2−F^-), and eq 2 cannot be directly used to fit the experimental data. As proposed by Azria et al., the differential cross section σ_{DEA} is generally in a proportion of[25]

$$|< \text{TNI state}|\text{partial wave}|\text{neutral state} >|^2 \quad (3)$$

As shown in Figure 1, if the impulsive dissociation $NF_3^- \rightarrow NF_2 + F^-$ is quite fast and the initial structure (C_{3v} symmetry) of the neutral is not deformed, then the TNI state in eq 3 is ^2E; on the other hand, the electron capture at the double-degenerate 5e orbital usually leads to the structural deformation due to the Jahn−Teller effect. The vibrationally inelastic collision study of $e^- + NF_3$ has indicated that the symmetric (υ_1) and asymmetric (υ_3) stretching modes were predominant around the electron energy 3 eV.[11] Accordingly, the structure of the stable NF_3^- was predicted to be in C_s symmetry with an elongated N−F bond.[5] If the dissociation is along this elongated N−F bond, the TNI state used in eq 3 should be $^2A'$, which is the low-lying Jahn−Teller split state of the ^2E resonant state. These two symmetries, E and A′, will be used, respectively, in the experimental data fitting with eq 3. For E symmetry, the partial waves p, d, and f are adopted; whereas the partial waves s, p, and d are considered for A′ symmetry.

In Figure 6, the angular distributions are obtained by the experimental data integrals for the selected annular area in each image of Figures 2 and 3. The selected annular covers the highest intensities of the fast F^- and corresponds to the kinetic energies in a range of 0.8 to 1.4 eV. The nonlinear least-squares fittings with eq 3 are performed for the measured data (the points). At the electron energy 0.5 eV, four sets of trial fittings are p + d (E) (blue dotted line), p + d + f (E) (red line), s + p (A′) (green line), and *s* + p +d (A′) (black line). The worst fitting shows the line obtained with the partial wave combination of s + p (A′), whereas the line with p + d (E) is almost the same as that with p + d + f (E), and thus the blue line (for the former) is covered by the red line (the latter). The best one is the line obtained with the s + p +d (A′) set. Two sets of the data fittings, p + d + f (E) and s + p + d (A′), are used for the experimental data at the other six energies. In general, the fitting lines by s + p + d (A′) are better than those by p + d + f (E), but at 4.0 eV, the p + d + f (E) can reproduce much better not only the profiles but also the maximal

dx.doi.org/10.1021/jp400026c | J. Phys. Chem. A 2013, 117, 3176−3182

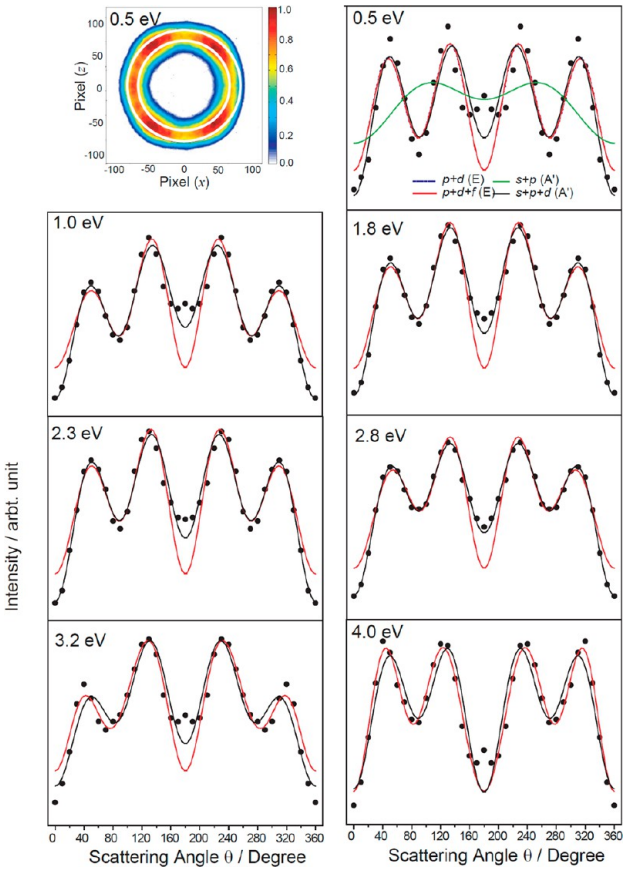

Figure 6. Angular distributions of the fast F^- fragment that are obtained by the integral of signals in the white annular area. (See the upper left panel for the image recorded at the electron attachment energy 0.5 eV.) The annular area covers the signals of the anion with the kinetic energies between 0.8 and 1.4 eV. The ion intensity is normalized, respectively, at each electron energy.

positions of the angular distributions. The improvement by using p + d + f (E) can also be found as the gradual increase in the fitting correlation values R^2 listed in Table 2. This supports

Table 2. Ratios of Partial Wave Contributions and the R^2 Values for the Fits of the Angular Distribution of F^-[a]

	E symmetry (p + d + f)		A′ symmetry (s + p + d)	
attachment energy	a_p:a_d:a_f	R^2	a_s:a_p:a_d	R^2
0.5 eV	1.00:1.59:0.02	0.74	1.00:0.44:1.82	0.85
1.0 eV	1.00:1.46:0.13	0.79	1.00:0.64:1.25	0.96
1.8 eV	1.00:1.24:0.07	0.87	1.00:0.79:1.53	0.98
2.3 eV	1.00:1.21:0.07	0.85	1.00:0.56:1.55	0.97
2.8 eV	1.00:1.08:0.10	0.87	1.00:0.53:1.56	0.99
3.2 eV	1.00:1.62:0.44	0.84	1.00:0.54:1.00	0.90
4.0 eV	1.00:1.11:0.15	0.95	1.00:0.38:2.46	0.88

[a]Here a is the weighing coefficient of the corresponding partial wave.

our assumption mentioned above that with the increase in the electron attachment energy the TNI may decompose more quickly. Therefore, NF_3^- (^2E) formed at the higher energy electron will quickly decompose while the initial C_{3v} symmetry structure is nearly maintained before the fragmentation. For the lower electron energies, the structural deformation ($C_{3v} \rightarrow C_s$) due to the Jahn–Teller effect occurs first; then, the N–F bond in NF_3^- (A′) is broken. In Table 2, the contributions of the different partial waves can be found as the ratios, a_p:a_d:a_f for E symmetry and a_s:a_p:a_d for A′ symmetry, indicating that the d partial waves for E and A′ symmetries are more important than those with the lower angular momenta [l = 0 (s), 1(p)].

3.4. Perfluorination Effect. The perfluorination effect on the DEA process is addressed here by a comparison between the present work and the anion velocity image study of the DEA to NH_3.[6] The similar effect was reported for the total cross sections of the electron collisions with NF_3 and NH_3, exhibiting the significant differences in the electron energy range of 1–10 eV.[13] Two resonant states, $^2A_1$ (5.5 eV) and ^2E (10.5 eV), of NH_3^- were proposed in this energy range (see ref 6 and references cited in); NF_3^- has two similar resonant states but in the reversed energy sequence. Because only the lowest resonant state ^2E of NF_3^- is discussed here, we compare the DEA processes at the ^2E state between these two TNIs. For NH_3^-, the two-body dissociation to H^- and NH_2^- exhibited the forward (H^-) and backward (NH_2^-) distributions, implying a molecular orientation effect in the DEA process.[6] The molecular orientation effect was observed more clearly in another study of the DEA to CF_4.[18] However, this phenomenon is not present for NF_3, perhaps due to the different shapes of the related orbitals: 1e (NH_3, see figure 8b in ref 6) and 5e (NF_3, see figure 5). The unsatisfied experimental data fittings using p + d (E) for the angular distributions of H^- and NH_2^- reminded the authors that the Jahn–Teller effect or nonadiabatic effect should be considered.[6] Here two sets of the fittings with E and A′ symmetries are examined. We find that the Jahn–Teller effect may be more predominant at the lower electron energy, but this effect is much weaker at the higher energy, and the dissociation of TNI NF_3^- should be extremely fast. The better experimental data fitting with E symmetry than that with A′ symmetry at 4.0 eV also implies that in this energy range the two-body dissociation is still related to the ^2E state (NF_3^-) while the three-body dissociation is related to the $^2A_1$ resonant state (NF_3^{*-}). This is in accord with the previous conclusion.[5] NH^- as the minor could be produced via the three-body dissociation $NH_3^- \rightarrow NH^-(^2\Pi) + H + H$, but it could be mixed into the image of NH_2^- because these two anions were not separated well in the experiments due to their close masses ($m(NH^-)$ = 13 amu, $m(NH_2^-)$ = 14 amu) and the limited resolution of the ion mass spectroscopy.[6] Here the three-body dissociation to $NF(X\ ^3\Sigma^-) + F + F^-$ can be affirmatively assigned as the source of the slow F^- observed in the images at 1.8 and 2.3 eV.

4. CONCLUSIONS

The low-energy (0.5 to 4.5 eV) electron dissociative attachments to NF_3 are investigated by the anion sliced velocity imaging spectroscopy. The kinetic and angular distributions of the F^- fragment indicate that there are two distinctly different channels, namely, two-body and three-body fragmentations at the higher electron attachment energies. The anisotropic distributions of the fast F^- anions are interpreted as the two-body dissociations at the ^2E resonant state of NF_3^- as well as its Jahn–Teller split state $^2A'$. Furthermore, we suggest that with the increase in the electron attachment energy, the Jahn–Teller effect decays; meanwhile, the dissociation of NF_3^- becomes much faster. At the electron energies 1.8 and 2.3 eV, the slow F^- ions are observed as the central signals in the sliced images and assuredly assigned as the products from the three-body dissociation to $NF(X\ ^3\Sigma^-) + F + F^-$. Both of the three-body dissociations $NF + F + F^-$ and $N + F_2 + F^-$ may be involved at

dx.doi.org/10.1021/jp400026c | J. Phys. Chem. A 2013, 117, 3176–3182

the higher electron attachment energies 4.0 and 4.5 eV, and the anisotropic distributions of the slow F^- produced in the above two three-body channels show some differences.

AUTHOR INFORMATION

Corresponding Author

*Tel: +86-551-63606465. E-mail: sxtian@ustc.edu.cn.

Notes

The authors declare no competing financial interest.

ACKNOWLEDGMENTS

This work is supported by MOST (Grant No. 2013CB834602), NSFC (Grant No. 21273213), and FRFCU.

REFERENCES

(1) *Electron Molecule Interactions and Their Applications*; Christophorou, L. G., Ed.; Academic: New York, 1984.

(2) Illenberger, E.; Momigny, J. *Gaseous Molecular Ions*; Springer: New York, 1992.

(3) Harland, P. W.; Franklin, J. L. Partitioning of Excess Energy in Dissociative Resonance Capture Processes. *J. Chem. Phys.* **1974**, *61*, 1621−1636.

(4) (a) Nandi, D.; Rangwala, S. A.; Kumar, S. V. K.; Krishnakumar, E. *Int. J. Mass Spectrom.* **2001**, *205*, 111−117. (b) Nandi, D.; Krishnakumar, E. Dissociative Electron Attachment to Polyatomic Molecules: Ion Kinetic Energy Measurements. *Int. J. Mass Spectrom.* **2010**, *289*, 39−46.

(5) Ruckhaberle, N.; Lehmann, L.; Matejcik, S.; Illenberger, E.; Bouteiller, Y.; Periquet, V.; Museur, L.; Desfrançois, C.; Schermann, J.-P. Free Electron Attachment and Rydberg Electron Transfer to NF_3 Molecules and Clusters. *J. Phys. Chem. A* **1997**, *101*, 9942−9947.

(6) Ram, N. B.; Krishnakumar, E. Dissociative Electron Attachment Resonances in Ammonia: A Velocity Slice Imaging Based Study. *J. Chem. Phys.* **2012**, *136*, 164308.

(7) (a) Schulz, M.; Moshammer, R.; Fisher, D.; Kollmus, H.; Madison, D. H.; Jones, S.; Ullrich, J. Three-Dimensional Imaging of Atomic Four-Body Processes. *Nature* **2003**, *422*, 48−50. (b) Strasser, D.; Lammich, L.; Krohn, S.; Lange, M.; Kreckel, H.; Levin, J.; Schwalm, D.; Vager, Z.; Wester, R.; Wolf, A.; Zajfman, D. Two- and Three-Body Kinematical Correlation in the Dissociative Recombination of H_3^+. *Phys. Rev. Lett.* **2001**, *86*, 779. (c) Laperle, C. M.; Mann, J. E.; Clements, T. G.; Continetti, R. E. Three-Body Dissociation Dynamics of the Low-lying Rydberg States of H_3 and D_3. *Phys. Rev. Lett.* **2004**, *93*, 153202.

(8) (a) Savee, J. D.; Mozhayskiy, V. A.; Mann, J. E.; Krylov, A. I.; Continetti, R. E. The Role of Excited-State Topology in Three-body Dissociation of *Sym*-triazine. *Science* **2008**, *321*, 826−830. (b) Crider, P. E.; Harrson, A. W.; Neumark, D. M. Two- and Three-Body Photodissociation Dynamics of Diiodobromide (I_2Br^-) Anion. *J. Chem. Phys.* **2011**, *134*, 134306.

(9) Haxton, D. J.; Rescigno, T. N.; McCurdy, C. W. Three-Body Breakup in Dissociative Electron Attachment to the Water Molecule. *Phys. Rev. A* **2008**, *78*, 040702R.

(10) Wu, B.; Xia, L.; Li, H.-K.; Zeng, X.-J.; Tian, S. X. Positive/Negative Ion Velocity Mapping Apparatus for Electron-Molecule Reactions. *Rev. Sci. Instrum.* **2012**, *83*, 013108.

(11) Boesten, L.; Tachibana, Y.; Nakano, Y.; Shinohara, T.; Tanaka, H.; Dillon, M. A. Vibrationally Inelastic and Elastic Cross Sections for e + NF_3 Collisions. *J. Phys. B* **1996**, *29*, 5475−5491.

(12) Joucoski, E.; Bettega, M. H. F. Elastic Scattering of Low-Energy Electrons by NF_3. *J. Phys. B* **2002**, *35*, 783−793.

(13) Szmytkowski, C.; Domaracka, A.; Możejko, P.; Ptasińska-Denga, E.; Kłosowski, Ł.; Piotrowicz, M.; Kasperski, G. Electron Collisions with Nitrogen Trifluoride (NF_3) Molecules. *Phys. Rev. A* **2004**, *70*, 032707.

(14) Christophorou, L. G.; Olthoff, J. K. *Fundamental Electron Interactions with Plasma Processing Gases*; Kluwer/Plenum: New York, 2004.

(15) Seccombe, D. P.; Jarvis, G. K.; Fisher, B. O.; Tuckett, R. P. Fragmentation of the Valence Electronic States of NF_3^+ Studied by Threshold Photoelectron-Photoion Coincidence Spectroscopy. *Chem. Phys.* **1999**, *250*, 335−346.

(16) Wu, B.; Xia, L.; Wang, Y.-F.; Li, H.-K.; Zeng, X.-J.; Tian, S. X. Renner-Teller Effect on Dissociative Electron Attachments to Carbon Dioxide. *Phys. Rev. A* **2012**, *85*, 052709.

(17) Xia, L.; Wu, B.; Li, H.-K.; Zeng, X.-J.; Tian, S. X. Communication: Imaging the Indirect Dissociation Dynamics of Temporary Negative Ion: $N_2O^- \rightarrow N_2 + O^-$. *J. Chem. Phys.* **2012**, *137*, 151102.

(18) Xia, L.; Zeng, X.-J.; Li, H.-K.; Wu, B.; Tian, S. X. Orientation Effect in the Low-Energy Electron Attachment to the Apolar Carbon Tetrafluoride Molecule. *Angew. Chem., Int. Ed.* **2013**, *52*, 1013−1016.

(19) Miller, T. M.; Friedman, J. F.; Williamson, J. S.; Schaffer, L. C.; Viggiano, A. A. A New Instrument for Thermal Electron Attachment at High Temperature: NF_3 and CH_3Cl Attachment Rate Constants up to 1100 K. *Rev. Sci. Instrum.* **2009**, *80*, 034104.

(20) Haney, M. A.; Franklin, J. L. Correlation of Excess Energies of Electron-impact Dissociations with the Translational Energies of the Products. *J. Chem. Phys.* **1968**, *48*, 4093−4097.

(21) Tronc, M.; Fiquet-Fayard, F.; Schermann, C.; Hall, R. I. Differential Cross Sections and Angular Distributions of H^- from Dissociative Electron Attachment to H_2 Between 3.75 and 13 eV. *J. Phys. B* **1977**, *10*, 305−321.

(22) O'Malley, T. F.; Taylor, H. S. Angular Dependence of Scattering Products in Electron-Molecule Resonant Excitation and in Dissociative Attachment. *Phys. Rev.* **1968**, *176*, 207−221.

(23) Dunn, G. H. Anisotropies in Angular Distributions of Molecular Dissociation Products. *Phys. Rev. Lett.* **1962**, *8*, 62−64.

(24) Ómarsson, F. H.; Ingólfsson, O.; Mason, N. J.; Krishnakumar, E. Dissociative Electron Attachment to CF_3Cl. *Eur. J. Phys. D* **2012**, *66*, 51.

(25) Azria, R.; Coat, Y. L.; Lefevre, G.; Simon, D. Dissociative Electron Attachment on H_2S: Energy and Angular Distributions of H^- Ions. *J. Phys. B* **1979**, *12*, 679−687.